ChemPhysChem

Research Article
doi.org/10.1002/cphc.202300510

Chemistry Europe
European Chemical Societies Publishing

www.chemphyschem.org

Special Collection

Bromine Adsorption and Thermal Stability on Rh(111): A Combined XPS, LEED and DFT Study

Eva Marie Freiberger,[a] Julien Steffen,[b] Natalie J. Waleska-Wellnhofer,[a] Anton Harrer,[a] Felix Hemauer,[a] Valentin Schwaab,[a] Andreas Görling,[b] Hans-Peter Steinrück,[a] and Christian Papp*[a, c]

This study addresses a fundamental question in surface science: the adsorption of halogens on metal surfaces. Using synchrotron radiation-based high-resolution X-ray photoelectron spectroscopy (XPS), temperature-programmed XPS, low-energy electron diffraction (LEED) and density functional theory (DFT) calculations, we investigated the adsorption and thermal stability of bromine on Rh(111) in detail. The adsorption of elemental bromine on Rh(111) at 170 K was followed *in situ* by XPS in the Br 3d region, revealing two individual, coverage-dependent species, which we assign to fcc hollow- and bridge-bound atomic bromine. In addition, we find a significant shift in binding energy upon increasing coverage due to adsorbate-adsorbate interactions. Subsequent heating shows a high thermal stability of bromine on Rh(111) up to above 1000 K, indicating strong covalent bonding. To complement the XPS data, LEED was used to study the long-range order of bromine on Rh(111): we observe a $(\sqrt{3}\times\sqrt{3})R30^\circ$ structure for low coverages ($\leq$0.33 ML) and a star-shaped compression structure for higher coverages (0.33–0.43 ML). Combining LEED and DFT calculations, we were able to visualize bromine adsorption on Rh(111) in real space for varying coverages.

Introduction

A profound understanding of the interaction between halogens and metal surfaces on the molecular level is highly important for all on-surface processes, in which halogens are involved as a reactant, by-product or promoter. This plays, for example, an important role in on-surface synthesis, in which precursor molecules adsorbed on a substrate are coupled to build up larger nanostructures with atomic precision.[1] In this context, coupling reactions with halogens as the leaving group are a popular synthetic route,[2] resulting in accumulation of the halogen on the respective surface, which might hinder proper continuation of the on-surface synthesis.[3] Also in electrochemistry, halogen adsorption on the metal electrodes can occur when using halogen-containing electrolytes, which might strongly influence the performance of the electrode. Thus, halogen interaction with metal surfaces is of tremendous interest for electrochemical research.[4] Moreover, halogens may act as promoters in heterogeneous catalysis, e.g., in the silver-catalyzed epoxidation of ethylene.[5]

In the past, numerous experimental and theoretical surface science studies on the adsorption of halogens on various different metal surfaces have been reported, such as Pt(111),[6] Pt(100),[6b] Pt(110),[7] Pd(111),[6c,8] Pd(110),[7] Ni(111),[9] Ni(110),[7,10] Cu(111),[11] Ag(111),[12] Au(111),[13] Au(100),[14] Fe(100)[15] and V(100).[16] In the experimental works, mostly low-energy electron diffraction (LEED), scanning tunneling microscopy (STM), temperature-programmed desorption (TPD) and work function measurements were employed. However, high-resolution X-ray photoelectron spectroscopy (XPS) data regarding the adsorption of halogens on metal surfaces, which we expect to be a very suitable tool to obtain detailed information regarding the adsorption behavior, can hardly be found. So far, only the interaction of chlorine and iodine with the Rh(111) surface has been investigated[17] while, to the best of our knowledge, the adsorption of bromine on Rh(111) has not yet been properly studied by means of surface science.

In this study, we investigated the adsorption and thermal stability of elemental bromine on the Rh(111) single-crystal surface *in situ* by synchrotron radiation-based high-resolution XPS and temperature-programmed XPS (TPXPS). Complementary LEED measurements were conducted to elucidate the long-range order of atomic bromine on Rh(111). In addition, density functional theory (DFT) was used to access adsorption energies

[a] E. M. Freiberger, N. J. Waleska-Wellnhofer, A. Harrer, F. Hemauer, V. Schwaab, Prof. Dr. H.-P. Steinrück, Prof. Dr. C. Papp
Physikalische Chemie II
Friedrich-Alexander-Universität Erlangen-Nürnberg
Egerlandstr. 3, 91058 Erlangen (Germany)
E-mail: christian.papp@fau.de

[b] Dr. J. Steffen, Prof. Dr. A. Görling
Theoretische Chemie
Friedrich-Alexander-Universität Erlangen-Nürnberg
Egerlandstr. 3, 91058 Erlangen (Germany)

[c] Prof. Dr. C. Papp
Physikalische und Theoretische Chemie
Freie Universität Berlin
Arnimallee 22, 14195 Berlin (Germany)
Homepage: www.bcp.fu-berlin.de/chemie/chemie/forschung/PhysTheoChem/agpapp/index.html

Supporting information for this article is available on the WWW under https://doi.org/10.1002/cphc.202300510

Special Collection An invited contribution to a Special Collection on Synchrotron-Based Photo- and Physical Chemistry

and to visualize the adsorption sites for varying surface coverages. We provide a comprehensive insight into the Br/Rh(111) system, thereby contributing to a molecular-level understanding of on-surface processes involving halogens.

Experimental

The XPS, TPXPS and LEED experiments were performed in a transportable two-chamber UHV apparatus, described in detail elsewhere,[18] which is *inter alia* equipped with a hemispherical electron analyzer, a micro-capillary array dosing system and LEED optics. The setup allows for manipulation of the sample along three axes and around two angles as well as for cooling of the sample to ~100 K using liquid nitrogen. Heating is done either resistively up to 1400 K or by a tungsten filament, mounted behind the sample, up to ~550 K. For temperature reading, K-type thermocouples are spotwelded directly to the sample.

We used a Rh(111) single crystal (MaTeck) as the substrate, which was cleaned by several cycles of Ar^+ sputtering, annealing to 1200 K and oxygen treatment at 900 K. Prior to the experiments, the crystal was checked for impurities by XPS. Elemental bromine, purchased from Merck Millipore and purified by several freeze-pump-thaw cycles, was dosed onto the sample using the micro-capillary array dosing system, whereby the Rh(111) sample was held at 170 K to avoid water co-adsorption. The exposure of bromine, calculated from the Br_2 background pressure in the chamber and the exposure time, is given in Langmuir (L, 1 L = 1.33×10^{-6} mbar s). The surface coverage was calibrated referring to LEED.

The adsorption and thermal stability of bromine on Rh(111) was probed *in situ* by XPS and TPXPS experiments, using synchrotron radiation provided by the open-port undulator beamline U49/2-PGM1[19] at the electron storage ring BESSY II of the Helmholtz Zentrum Berlin (HZB). During adsorption and subsequent heating, XP spectra were continuously collected in the Br 3d region. Between each spectrum, the sample was shifted by about 0.1 mm (larger than the X-ray diameter) to avoid beam damage. For the TPXPS, the sample was heated up to 550 K using the tungsten filament with a heating ramp of 0.5 K/s. Above 550 K, the filament was turned off and the sample was heated resistively. All spectra were recorded in normal emission. For the Br 3d and Rh $3d_{5/2}$ regions, photon energies of 170 and 380 eV were chosen, leading to an overall energy resolution of 180 ± 20 and 220 ± 20 meV, respectively. In all XP spectra, the binding energies were referenced with respect to the Fermi edge and a linear background was subtracted. Peak fitting was performed using a convolution of Gaussian and Doniach-Šunjić functions. Additional laboratory-based XPS experiments using Mg K_α radiation (1253.6 eV) were performed in the course of the LEED study.

Periodic DFT calculations of the systems were carried out with the VASP code, using a plane wave basis set for the description of the valence electrons combined with the projector augmented wave (PAW) method for the representation of atomic cores.[20] The kinetic energy cutoff was set to 300 eV for the geometry relaxations of pristine rhodium slabs and for the optimizations of bromine adsorption positions. Exchange correlation effects were treated with the PBE functional.[21] The Grimme DFT–D3 dispersion correction scheme with Becke-Johnson damping was used for a better description of dispersion interactions.[22] The sampling of the Brillouin zone for the four considered adsorption scenarios (patterns 1–4) was done with the following settings: a Γ-containing 10×10×1 k-point mesh for pattern 1, a Γ-containing 4×4×1 k-point mesh for pattern 2, a Γ-containing 12×4×1 k-point mesh for pattern 3 and a Γ-containing 5×5×1 k-point mesh for pattern 4. Electronic states were smeared with the Methfessel-Paxton scheme (first order) and a broadening of 0.15 eV.[23]

The Rh(111) surface was modeled by six-layered surface slabs. The cell sizes were determined by an initial optimization of a rhodium bulk cell containing four atoms (Γ-containing 20×20×20 k-point mesh), and the distances between the atoms were taken to build up the initial surface slabs. The cell vectors and the bottom three metal atom layers were held fixed during the following calculations. The surface slabs were cut from a large orthogonal unit cell with the new Fortran program "cut unitcell", designed for this purpose. Bromine atoms were placed initially either on top, bridge, or fcc/hcp hollow positions. The geometries were optimized until all Cartesian force components were below 0.02 eV/Å. For the determination of adsorption energies, an isolated bromine molecule was optimized as reference in a unit cell of 30×30×30 Å size with a Γ-only sampling of the Brillouin zone. Adsorption energies were calculated by subtracting the energy of the clean rhodium surface and the energy of the appropriate number (number of bromine atoms in the unit cell *n*) of free bromine atoms (energy of the free bromine molecule divided by two) from the energy of the optimized unit cell of *n* bromine atoms adsorbed on Rh(111) (Equation 1). For all four adsorption scenarios (patterns 1–4), the energies were translated into the effective (average) energy to adsorb one bromine atom in the actual pattern.

$$E_{ads}(Br) = \frac{E(n\ Br/Rh(111)) - E(Rh(111)) - n\ \frac{E(Br_2)}{2}}{n} \quad (1)$$

Results and Discussion

First, we address the adsorption of bromine on the Rh(111) surface. Elemental bromine was dosed onto the substrate held at 170 K via background exposure until saturation (0.15 L; 0.43 ML). Bromine arrives at the surface presumably as diatomic molecule. However, according to literature, halogens adsorb on metal surfaces in general in a dissociative manner.[24] Thus, we assume in the following that only bromine atoms adsorb on Rh(111). The adsorption process was followed *in situ* by high-resolution XPS in the Br 3d region. Figures 1a and 1b provide the spectra acquired during adsorption as a waterfall plot and fits of the Br 3d spectra at selected coverages, respectively. Table S1 in the Supporting Information (SI) contains the respective fit parameters.

Upon bromine adsorption on Rh(111), two peaks evolve at 68.90/69.94 eV, which are assigned to the spin-orbit-split Br $3d_{3/2}$ and $3d_{5/2}$ doublet of a single bromine species. Up to a coverage of ~0.23 ML (yellow in Figure 1a), the signal intensity of the doublet increases continuously, and the peak positions remain roughly constant. Figure 1b (bottom) provides a fit of the spectrum at an atomic bromine coverage of 0.23 ML (yellow doublet). For peak fitting, the signal intensity ratio (2 : 3) and splitting (1.04 eV) between Br $3d_{3/2}$ and $3d_{5/2}$ were always kept constant. With further bromine exposure, a significant shift of the yellow doublet of about 0.30 eV to lower binding energies occurs, which is attributed to strong adsorbate-adsorbate interactions. Furthermore, a second doublet at 68.18/69.22 eV emerges (orange in Figure 1a), indicating the development of a second bromine species at higher coverages. The signals

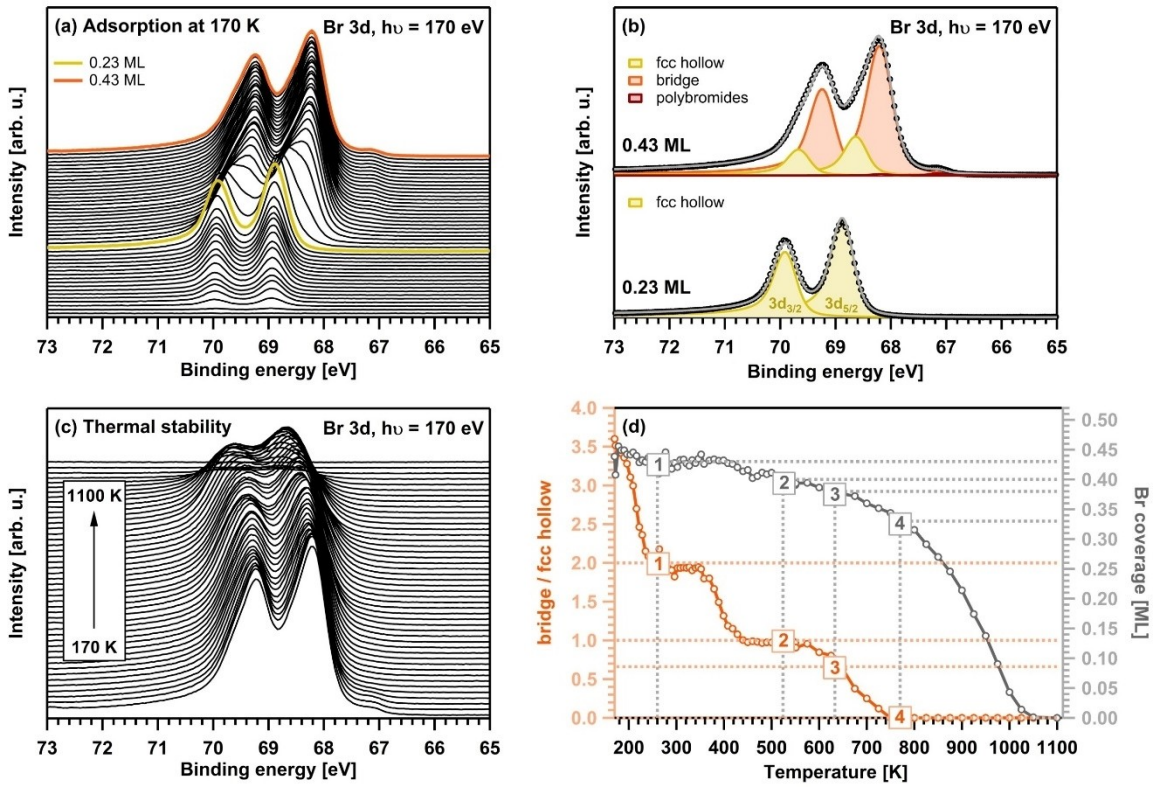

Figure 1. (a) Waterfall plot of the Br 3d spectra acquired during the adsorption of 0.15 L elemental bromine on a clean Rh(111) surface; coverages of 0.23 and 0.43 ML are marked yellow and orange, respectively. (b) Fits of the Br 3d spectra at 0.23 (bottom) and 0.43 ML (top); each bromine species leads to a doublet in the spectrum due to spin orbit splitting (Br $3d_{3/2}$:Br $3d_{5/2}$ = 2:3). (c) Waterfall plot of the Br 3d spectra acquired during heating of 0.43 ML Br/Rh(111) from 170 to 1100 K. (d) Analysis of the TPXPS experiment, showing the bromine coverage (gray curve) as well as the ratio between fcc hollow- and bridge-bound bromine atoms (orange curve) in dependance of the annealing temperature. The main desorption takes place between 800 and 1000 K. The numbers 1–4 correspond to the four different LEED patterns found for Br/Rh(111) at varying coverages.

saturate after a bromine exposure of ~0.11 L; the saturation coverage corresponds to about 0.43 ML, as derived from our LEED measurements and DFT calculations discussed below. This is in good agreement with the saturation coverage of bromine on Cu(111), 0.42 ML,[11a] considering that Rh(111) and Cu(111) have similar surface lattice constants (2.69 vs. 2.56 Å[25]). In Figure 1b (top), a fit of the Br 3d spectrum after an exposure of 0.15 L is shown, in which the new doublet is colored orange. In addition, a third very small contribution at even lower binding energies (67.13/68.17 eV) is observed (red doublet). This doublet gains intensity only for very high bromine exposures. In Figure S1 in the SI, a Br 3d spectrum after the exposure of Rh(111) to ~160 L of bromine (at ~10^{-4} mbar) is depicted, in which this additional contribution is clearly visible. We tentatively assign this additional species to the formation of polybromides at higher exposures/higher pressures. In summary, the *in situ* adsorption experiment reveals the existence of two individual, coverage-dependent bromine species on the Rh(111) surface. According to LEED and DFT (see below), we suggest these two species to belong to bromine adsorbed on different adsorptions sites: fcc hollow sites for low coverages up to 0.33 ML and fcc hollow as well as bridge sites for higher coverages. Moreover, the observed peak shift indicates strong adsorbate-adsorbate interactions upon increasing coverage, due to displacement from the optimum adsorption sites at high coverages.

Next, the thermal stability of bromine adsorbed on Rh(111) was investigated by TPXPS in a temperature range between 170 and 1100 K. The Br 3d spectra recorded during heating are depicted as a waterfall plot in Figure 1c. Upon heating, a shift to higher binding energies takes place, which results from a decreasing signal intensity of the orange bromine species at 68.18/69.22 eV. The individual XP spectra are, however, difficult to fit due to the overlap of the two doublets and additional peak broadening with increasing temperature. The fit parameters are listed in Table S1 in the SI. For the fcc hollow and bridge species, an increase of the Gaussian width from 0.38 to 0.89 eV and 0.40 to 0.55 eV was observed, respectively. The broadening can be explained by thermally induced disorder of the bromine layer on Rh(111), which leads to a statistical displacement from the optimum adsorption sites and correspondingly slightly different XPS binding energies. Upon heating, the translation of bromine atoms on the surface is excited, i.e., the atoms may change from one adsorption site to another. The signal assigned to polybromides vanishes at ~220 K, indicating a rather low stability of the polybromides. Figure 1d provides the quantitative analysis of the surface coverage during the TPXPS experiment (gray curve). It reveals a quite high thermal stability up to above 1000 K, which is a sign

of strong covalent bonding of bromine to the substrate. The orange curve in Figure 1d will be referred to in the last section of the manuscript. Please note that, in the adsorption as well as the TPXPS experiment, diffraction effects may influence the observed signal intensity to some extent since the photoelectrons have an energy of about 100 eV.

In addition to the Br 3d data, spectra in the Rh $3d_{5/2}$ region were collected prior to adsorption, after adsorption and after heating to 1100 K in the scope of the TPXPS experiment. The respective spectra and a brief discussion are provided in the SI (Figure S2).

To identify the two individual, coverage-dependent species observed in the Br 3d region during adsorption of bromine on Rh(111) (Figure 1b), complementary methods to XPS were needed. Hence, we performed LEED experiments and DFT calculations. For LEED, Rh(111) held at 170 K was exposed to 1.4 L elemental bromine to ensure saturation. All LEED images were taken at an electron energy of 160 eV and at temperatures below 170 K. Figure 2 provides the corresponding data.

Right after adsorption, the LEED image reveals no sharp diffraction spots other than the substrate spots (marked with yellow circles). Instead, we observe rather blurry, arched diffraction spots, which are attributed to arbitrary rotational domains. To induce order, we annealed the sample in 100 K steps. Upon annealing to 200 and 300 K, the LEED pattern hardly changes. Only after annealing to 400 K, a complex, "star-shaped" LEED pattern becomes visible, indicating a well-ordered adsorbate layer. In the SI, additional LEED images of this superstructure taken at electron energies of 180 and 265 eV are shown (Figure S3). Notably, we observe sharp diffraction spots only below 350 K. At higher temperatures, thermal motion leads to a bright background. This also fits the peak broadening observed in the TPXPS experiment.

The software LEEDpat4 provided by the Fritz Haber Institute of the Max Planck Society[26] allowed for interpretation of the LEED image. Using the basic 2D lattice group "hexagonal p31 m" and an angle of 60° between the substrate lattice vectors, we were able to simulate the LEED pattern observed after heating to 400 K. It is the superposition of the patterns of three symmetry-equivalent domains with commensurate sublattices, rotated to each other by 120°. They can be described by the following matrices: $\begin{pmatrix} 1 & 1 \\ -3 & 4 \end{pmatrix}$, $\begin{pmatrix} -2 & 1 \\ -1 & -3 \end{pmatrix}$ and $\begin{pmatrix} 1 & -2 \\ 4 & -1 \end{pmatrix}$.

When annealing to 500 K, the star-shaped pattern remains stable. At 600 K, a second slightly different star-shaped pattern is observed with some additional diffraction spots and overall smaller distances between the spots. This is probably due to the slowly decreasing surface coverage in this temperature range (see Figure 1d). According to a simulation in LEEDpat4, the new structure can also be described as a superposition of three domains of commensurate sublattices, that is, $\begin{pmatrix} 1 & 1 \\ -5 & 5 \end{pmatrix}$, $\begin{pmatrix} -2 & 1 \\ 0 & -5 \end{pmatrix}$ and $\begin{pmatrix} 1 & -2 \\ 5 & 0 \end{pmatrix}$.

Annealing to 700 K leads to a fundamental change of the superstructure. The new LEED pattern corresponds to a simple $(\sqrt{3}\times\sqrt{3})R30°$ superstructure. From the TPXPS data (Figure 1d) it can be seen that at these temperatures the surface coverage is already significantly lower. The $(\sqrt{3}\times\sqrt{3})R30°$ superstructure thus exists for lower bromine coverages while the star-shaped pattern evolves at higher bromine coverages towards saturation. Such a coverage-dependent change regarding the superstructure of halogens on a metal surface has already been observed, e.g., for the adsorption of chlorine and bromine on Cu(111)[11a,27] and the adsorption of chlorine on Ag(111).[12e] In these studies, halogen adsorption led to the formation of a $(\sqrt{3}\times\sqrt{3})R30°$ structure for low coverages, which changed to a more

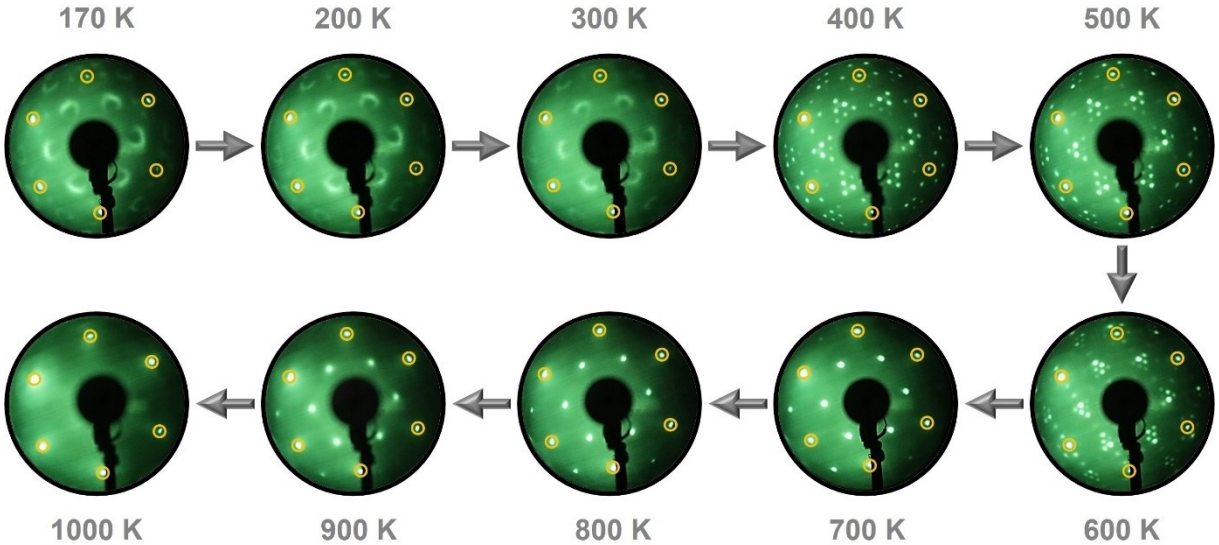

Figure 2. LEED images recorded at low temperatures (< 170 K) with an electron energy of 160 eV after adsorption of 1.4 L Br_2 on Rh(111) at 170 K and after subsequent heating to 1000 K in 100 K steps; the substrate diffraction spots are marked with yellow circles.

complex compression structure for coverages close to saturation.

On Rh(111), we find that the ($\sqrt{3}\times\sqrt{3}$)R30° superstructure remains stable up to 900 K. After heating to 1000 K, only the substrate diffraction spots are left. This indicates bromine desorption between 900 and 1000 K, which is perfectly in line with the TPXPS experiment (Figures 1c and 1d). To confirm these observations, we repeated this experiment. The respective LEED images are shown in Figure S4 in the SI. Here, we also observe the above-described two different star-shaped patterns and the transition to the ($\sqrt{3}\times\sqrt{3}$)R30° at 700 K. In addition, a third star-shaped LEED pattern can be found upon annealing to 600 K, characterized by even more diffraction spots and smaller distances ($\begin{pmatrix} 1 & 1 \\ -6 & 7 \end{pmatrix}$, $\begin{pmatrix} -2 & 1 \\ -1 & -6 \end{pmatrix}$ and $\begin{pmatrix} 1 & -2 \\ 7 & -1 \end{pmatrix}$).

Along with the LEED images, we recorded XP spectra in the Br 3d and 3p region. Please note that all XPS measurements referred to in the following are conducted using laboratory-based X-ray radiation (Mg K_α: 1253.6 eV), which leads to a significantly lower energy resolution in comparison to the synchrotron radiation-based data in Figure 1. In Figure 3a, the Br 3d spectra recorded after adsorption until saturation (0.43 ML) at 170 K (bottom; gray), after annealing to 400 K (center; orange) and after annealing to 700 K (top; yellow) are shown. Figure 3b presents the corresponding spectra in the Br 3p region. After adsorption at 170 K (gray curves in Figures 3a and 3b), no sharp diffraction spots are observed in LEED (Figure 3c). Upon annealing to 400 K (orange curves in Figures 3a and 3b), the signal intensity, i.e., surface coverage, and position remain virtually the same. Therefore, the corresponding star-shaped LEED pattern (Figure 3d) is assigned to the high-coverage/saturation scenario. Annealing to 700 K (yellow curves in Figures 3a and 3b), on the other hand, leads to a clear shift of ~0.8 eV to higher binding energies in both the Br 3p and Br 3d spectra. Moreover, the signal intensity decreases, i.e., the surface coverage is decreased (0.32 ML), due to bromine desorption. The shift and the lower signal intensity is explained by desorption of the high-coverage species observed in the

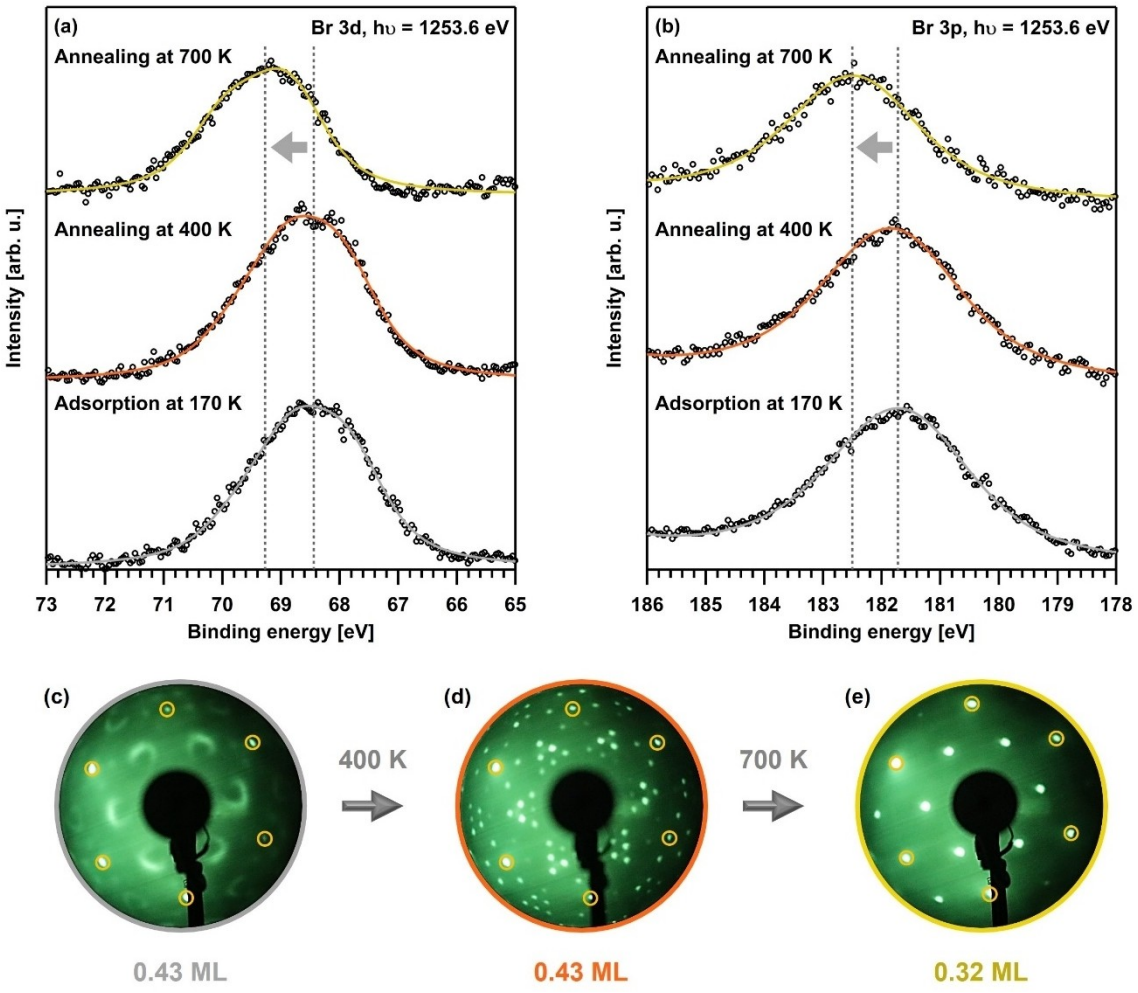

Figure 3. (a), (b) Laboratory-based XP spectra recorded after adsorption at 170 K (bottom; gray), annealing to 400 K (center; orange) and annealing to 700 K (top; yellow) in the Br 3d and 3p region, respectively; the gray dashed lines visualize the shift of the peak center to higher binding energies upon heating to 700 K. (c)–(e) Corresponding LEED images.

synchrotron radiation-based XPS experiments (Figure 1b, orange doublet). The yellow curve corresponds then solely to the low-coverage species in the *in situ* adsorption experiment in Figure 1b (yellow doublet). From this observation, we conclude that the $(\sqrt{3}\times\sqrt{3})R30^\circ$ superstructure observed upon annealing at 700 K (Figure 3e) belongs to the low-coverage species. The coverage-dependent shift in XPS thus seems to go along with the compression-induced change of the Br/Rh(111) superstructure from the $(\sqrt{3}\times\sqrt{3})R30^\circ$ to the star-shaped structure.

To support our assumption that the $(\sqrt{3}\times\sqrt{3})R30^\circ$ structure evolves for low-coverage adsorption, the clean Rh(111) surface, held at 170 K, was exposed to a smaller bromine dose of 0.06 L, and XPS as well as LEED were conducted (Figure S5 in the SI). The results indeed fit our expectations: The peak positions and coverages (0.27 ML) in the Br 3d and 3p XP spectra match with the low-coverage species as observed in the above-discussed synchrotron radiation- and laboratory-based experiments, and the corresponding LEED pattern reveals a $(\sqrt{3}\times\sqrt{3})R30^\circ$ superstructure. We suggest that bromine adsorbs in $(\sqrt{3}\times\sqrt{3})R30^\circ$ islands up to a surface coverage of 0.33 ML, at which the surface is fully covered. With further increasing coverage, compression of the overlayer occurs, and the star-shaped patterns evolve. Upon heating to 900 K (Figure S6 in the SI), the $(\sqrt{3}\times\sqrt{3})R30^\circ$ pattern is still observed. After heating to 1000 K, again only the substrate diffraction spots remain.

Overall, we observed four different LEED patterns, which are in the following referred to as patterns 1–4 (Figure 4). Using the software LEEDpat4, it was possible to simulate these LEED patterns, and the corresponding unit cells in real space were derived (Figure S7 in the SI). For the $(\sqrt{3}\times\sqrt{3})R30^\circ$ structure (pattern 1, Figure 4a), the real-space unit cell contains three rhodium atoms and one bromine atom, leading to a surface coverage of 0.33 ML. For the saturation coverage (pattern 4, Figure 4d), the real-space unit cell contains seven rhodium atoms, and the coverage equals n/7 ML. Taking our experimental observations into consideration, a coverage of $3/7 \approx 0.43$ ML is reasonable. Patterns 2 and 3 (Figures 4b and 4c) evolve upon the transition from pattern 4 to 1 due to bromine desorption, i.e., these relate to coverages between 0.43 and 0.33 ML. These considerations result in coverages of $5/13 \approx 0.38$ ML and $4/10 = 0.40$ ML for patterns 2 and 3, respectively. Based on the determined unit cells and coverages, we used DFT to calculate optimized structures for all four patterns in order to obtain the real-space structures for the four different coverages. Figure S7 in the SI shows a scheme describing this "translation" of the experimental LEED measurements into real-space models. The DFT-calculated structures are depicted in Figures S8–S11 in the

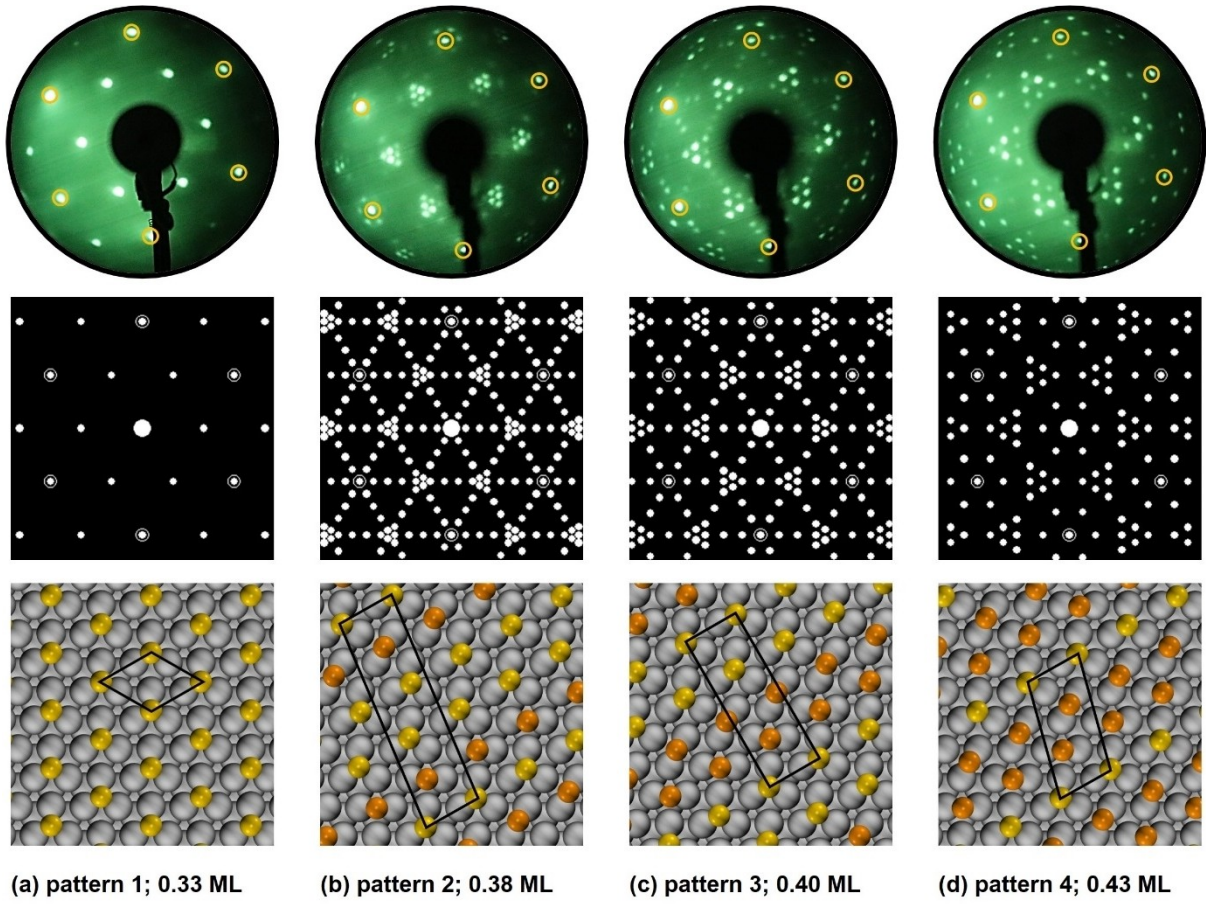

Figure 4. (a)–(d) Experimentally acquired LEED images of patterns 1–4 (substrate diffraction spots marked by yellow circles), corresponding simulated LEED patterns (reciprocal space) and therefrom derived real-space models. Bromine atoms on fcc hollow and bridge sites are colored yellow and orange, respectively. The unit cells are indicated in black.

SI. The absolute DFT energies of all patterns and the adsorption energies of bromine are listed in Table S2. Figure 4 provides the most stable patterns found for the four coverages, with the corresponding DFT energies being given in Table 1.

The calculations show that the fcc hollow site (−2.31 eV) is most favorable for bromine adsorption with the hcp hollow site being slightly less stable (−2.23 eV). For the bridge site, an adsorption energy of −2.18 eV was found. The on-top site (−1.76 eV) is by far the least stable. The same trend (fcc hollow > hcp hollow > bridge > on-top) regarding the adsorption energies has already been reported for bromine adsorption on Cu(111), Au(111), Pt(111) and Pd(111).[28] In the ($\sqrt{3}\times\sqrt{3}$)R30° structure (pattern 1; ≤0.33 ML), all the bromine atoms are located on fcc hollow sites (yellow bromine atoms in Figure 4). Increasing the coverage causes more and more bromine atoms to shift to the less stable bridge sites (orange bromine atoms in Figure 4). For pattern 2, 2/5 of the bromine atoms occupy bridge sites while 3/5 stay on the fcc hollow sites. For pattern 3, half of the bromine is bridge-bound. Eventually, for pattern 4 (saturation), 2/3 of the bromine atoms are bridge-bound while only 1/3 remains on the preferable fcc hollow sites. Please note that in patterns 2–4 the bromine atoms are not exactly located on the fcc hollow/bridge sites. Placing them directly on these sites is energetically less favorable. After structure relaxation, a minor distortion occurs as observed in Figures 4b–4d.

The DFT models help us to identify the two individual bromine species observed in the high-resolution XPS experiment. The low-coverage species (Figure 1b, yellow doublet) corresponds to bromine located on fcc hollow sites. The second species, which arises upon increasing the local coverage to above the one of the ($\sqrt{3}\times\sqrt{3}$)R30° structure (Figure 1b, orange doublet), is assigned to bromine shifted to bridge sites due to compression of the bromine overlayer. In Figure 1d, the ratio between the yellow (fcc hollow) and the orange (bridge) doublet is plotted against the annealing temperature. In a range of 250–350 K, the ratio equals approximately 2 and the coverage corresponds to ~0.43 ML. This perfectly agrees with the existence of pattern 4. Between 450 and 580 K, the ratio equals 1 and the coverage is ~0.40 ML, which fits pattern 3. At about 630 K, the coverage corresponds to 0.38 ML. Here, we observe a ratio of 0.66, correlating to pattern 2. At temperatures ≥770 K, the coverage is ≤0.33 ML, and all bromine atoms are adsorbed on fcc hollow sites in ($\sqrt{3}\times\sqrt{3}$)R30° islands, being in perfect accordance with pattern 1. The analysis of the ratio between the two different adsorption sites also allows for insights into the situation at low temperatures, where the rather blurry, arched diffraction spots are observed. The ratio of ~3.5 suggests that an even higher bridge population of ~78% is present on the surface, before ordered structures are formed.

Table 1. Absolute DFT energies as well as Br adsorption energies for the four most stable patterns.

scenario	$E(n\ Br/Rh(111))$ [eV]	$E_{ads}\ (Br)$ [eV]
pattern 1 (0.33 ML Br)	−139.49	−2.31
pattern 2 (0.38 ML Br)	−606.43	−2.17
pattern 3 (0.40 ML Br)	−466.88	−2.16
pattern 4 (0.43 ML Br)	−327.39	−2.10

Conclusions

XPS, TPXPS, LEED and DFT were utilized to investigate the adsorption and thermal stability of elemental bromine on the Rh(111) single-crystal surface. Synchrotron radiation-based high-resolution XPS allowed to study the low-temperature (170 K) adsorption of bromine on Rh(111) *in situ*. At low coverages, a single bromine species is observed, which is assigned to atomic bromine on fcc hollow adsorption sites. Upon increasing the surface coverage until saturation, a second species evolves that belongs to bridge-bound atomic bromine. Furthermore, strong adsorbate-adsorbate interaction causes a significant shift to lower binding energies. The thermal stability of up to above 1000 K derived from TPXPS indicates strong covalent bonding of bromine on Rh(111). Using LEED as a complementary method, we find different superstructures of bromine on Rh(111): a ($\sqrt{3}\times\sqrt{3}$)R30° superstructure for coverages ≤0.33 ML and more complex, star-shaped compression structures for coverages between 0.33 and 0.43 ML. DFT calculations, based on the knowledge derived from the LEED and XPS experiments, enabled us to visualize bromine adsorption on Rh(111) for different coverages in real space, which illustrates the compression-induced shift of atomic bromine from fcc hollow to bridge sites upon increasing the surface coverage.

In this study, the coverage-dependent compression of a halogen overlayer has been observed for Rh(111) for the first time. Also, we were able to prove the combination of high-resolution XPS, LEED and DFT to be very suitable to investigate the adsorption of halogen atoms on metal surfaces on the molecular level.

Supporting Information

The authors have cited additional references within the Supporting Information.[29]

Acknowledgements

Measurements were carried out at the BESSY II electron storage ring operated by the Helmholtz-Zentrum Berlin (HZB) für Materialien und Energie. We would like to thank HZB for the allocation of beamtime and the BESSY II staff for support during the beamtime. This work was funded by the DFG within SFB 953 "Synthetic Carbon Allotropes", project no. 182849149, and SFB 1452 "Catalysis at Liquid Interfaces", project no. 431791331. EMF and CP thank the Fonds der Chemischen Industrie for

financial support. Open Access funding enabled and organized by Projekt DEAL.

Conflict of Interests

The authors declare no conflict of interest.

Data Availability Statement

The data that support the findings of this study are available from the corresponding author upon reasonable request.

Keywords: adsorption sites · halogens on metals · high-resolution X-ray photoelectron spectroscopy · synchrotron radiation · LEED

[1] a) Q. Sun, R. Zhang, J. Qiu, R. Liu, W. Xu, *Adv. Mater.* **2018**, *30*, 1705630; b) S. Clair, D. G. de Oteyza, *Chem. Rev.* **2019**, *119*, 4717–4776.
[2] a) Q. Fan, J. M. Gottfried, J. Zhu, *Acc. Chem. Res.* **2015**, *48*, 2484–2494; b) D. Peyrot, F. Silly, *ACS Nano* **2016**, *10*, 5490–5498; c) M. Lackinger, *Chem. Commun.* **2017**, *53*, 7872–7885.
[3] J. Björk, F. Hanke, S. Stafström, *J. Am. Chem. Soc.* **2013**, *135*, 5768–5775.
[4] a) N. J. Tao, S. M. Lindsay, *J. Phys. Chem.* **1992**, *96*, 5213–5217; b) T. Yamada, K. Ogaki, S. Okubo, K. Itaya, *Surf. Sci.* **1996**, *369*, 321–335; c) O. M. Magnussen, B. M. Ocko, J. X. Wang, R. R. Adzic, *J. Phys. Chem.* **1996**, *100*, 5500–5508; d) O. Endo, D. Matsumura, K. Kohdate, M. Kiguchi, T. Yokoyama, T. Ohta, *J. Electroanal. Chem.* **2000**, *494*, 121–126; e) I. T. McCrum, S. A. Akhade, M. J. Janik, *Electrochim. Acta* **2015**, *173*, 302–309; f) Q. Zhu, S.-Q. Wang, *J. Electrochem. Soc.* **2016**, *163*, H796–H808.
[5] a) C. T. Campbell, *J. Catal.* **1986**, *99*, 28–38; b) B. Shen, Z. Fang, K. Fan, J. Deng, *Surf. Sci.* **2000**, *459*, 206–212; c) R. M. Lambert, R. L. Cropley, A. Husain, M. S. Tikhov, *Chem. Commun.* **2003**, 1184–1185; d) D. Torres, F. Illas, R. M. Lambert, *J. Catal.* **2008**, *260*, 380–383.
[6] a) E. Bertel, K. Schwaha, F. P. Netzer, *Surf. Sci.* **1979**, *83*, 439–452; b) T. E. Felter, A. T. Hubbard, *J. Electroanal. Chem. Interfacial Electrochem.* **1979**, *100*, 473–491; c) W. Erley, *Surf. Sci.* **1980**, *94*, 281–292; d) H. Xu, R. Yuro, I. Harrison, *Surf. Sci.* **1998**, *411*, 303–315.
[7] W. Erley, *Surf. Sci.* **1982**, *114*, 47–64.
[8] W. T. Tysoe, R. M. Lambert, *Surf. Sci.* **1982**, *115*, 37–47.
[9] a) W. Erley, H. Wagner, *Surf. Sci.* **1977**, *66*, 371–375; b) N. S. Komarov, T. V. Pavlova, B. V. Andryushechkin, *Surf. Sci.* **2016**, *651*, 112–119.
[10] a) T. W. Fishlock, J. B. Pethica, F. H. Jones, R. G. Egdell, J. S. Foord, *Surf. Sci.* **1997**, *377–379*, 629–633; b) T. W. Fishlock, J. B. Pethica, A. Oral, R. G. Egdell, F. H. Jones, *Surf. Sci.* **1999**, *426*, 212–224.
[11] a) R. G. Jones, M. Kadodwala, *Surf. Sci.* **1997**, *370*, L219–L225; b) J. Inukai, Y. Osawa, K. Itaya, *J. Phys. Chem. B* **1998**, *102*, 10034–10040; c) B. V. Andryushechkin, K. N. Eltsov, V. M. Shevlyuga, *Surf. Sci.* **2000**, *470*, L63–L68; d) B. V. Andryushechkin, V. V. Zheltov, V. V. Cherkez, G. M. Zhidomirov, A. N. Klimov, B. Kierren, Y. Fagot-Revurat, D. Malterre, K. N. Eltsov, *Surf. Sci.* **2015**, *639*, 7–12.
[12] a) P. J. Goddard, K. Schwaha, R. M. Lambert, *Surf. Sci.* **1978**, *71*, 351–363; b) D. J. Holmes, N. Panagiotides, D. A. King, *Surf. Sci.* **1989**, *222*, 285–295; c) D. D. Sneddon, A. A. Gewirth, *Surf. Sci.* **1995**, *343*, 185–200; d) O. Endo, H. Kondoh, T. Ohta, *Surf. Sci.* **1999**, *441*, L924–L930; e) B. V. Andryushechkin, V. V. Cherkez, B. Kierren, Y. Fagot-Revurat, D. Malterre, K. N. Eltsov, *Phys. Rev. B* **2011**, *84*, 205422; f) A. Seliverstov, D. Muzychenko, A. Volodin, E. Janssens, C. V. Haesendonck, *Surf. Sci.* **2023**, *734*, 122304.
[13] a) N. D. Spencer, R. M. Lambert, *Surf. Sci.* **1981**, *107*, 237–248; b) V. V. Zheltov, V. V. Cherkez, B. V. Andryushechkin, G. M. Zhidomirov, B. Kierren, Y. Fagot-Revurat, D. Malterre, K. N. Eltsov, *Phys. Rev. B* **2014**, *89*, 195425; c) V. V. Cherkez, V. V. Zheltov, C. Didiot, B. Kierren, Y. Fagot-Revurat, D. Malterre, B. V. Andryushechkin, G. M. Zhidomirov, K. N. Eltsov, *Phys. Rev. B* **2016**, *93*, 045432.
[14] E. Bertel, F. P. Netzer, *Surf. Sci.* **1980**, *97*, 409–424.
[15] a) P. A. Dowben, R. G. Jones, *Surf. Sci.* **1979**, *88*, 348–366; b) S. A. Saraireh, M. Altarawneh, M. A. Tarawneh, *Nanotechnol. Rev.* **2021**, *10*, 719–727.
[16] P. W. Davies, R. M. Lambert, *Surf. Sci.* **1980**, *95*, 571–586.
[17] a) M. P. Cox, R. M. Lambert, *Surf. Sci.* **1981**, *107*, 547–561; b) C. J. Barnes, A. Wander, D. A. King, *Surf. Sci.* **1993**, *281*, 33–41; c) A. G. Shard, V. R. Dhanak, A. Santoni, *Surf. Sci.* **1999**, *429*, 279–286.
[18] R. Denecke, M. Kinne, C. M. Whelan, H.-P. Steinrück, *Surf. Rev. Lett.* **2002**, *09*, 797–801.
[19] Helmholtz-Zentrum Berlin für Materialien und Energie, *JLSRF* **2016**, *2*, A72.
[20] a) G. Kresse, J. Furthmüller, *Phys. Rev. B* **1996**, *54*, 11169–11186; b) G. Kresse, J. Furthmüller, *Comput. Mater. Sci.* **1996**, *6*, 15–50; c) G. Kresse, D. Joubert, *Phys. Rev. B* **1999**, *59*, 1758–1775.
[21] J. P. Perdew, K. Burke, M. Ernzerhof, *Phys. Rev. Lett.* **1996**, *77*, 3865–3868.
[22] a) S. Grimme, J. Antony, S. Ehrlich, H. Krieg, *J. Chem. Phys.* **2010**, *132*, 154104; b) S. Grimme, S. Ehrlich, L. Goerigk, *J. Comput. Chem.* **2011**, *32*, 1456–1465.
[23] M. Methfessel, A. T. Paxton, *Phys. Rev. B* **1989**, *40*, 3616–3621.
[24] B. V. Andryushechkin, T. V. Pavlova, K. N. Eltsov, *Surf. Sci. Rep.* **2018**, *73*, 83–115.
[25] W. M. Haynes, D. R. Lide, T. J. Bruno, *CRC Handbook of Chemistry and Physics*, 95 ed., CRC Press, Boca Raton, **2014**, 12-6–12-17.
[26] K. E. Hermann (FHI), M. A. Van Hove (HKBU), LEEDpat, Version 4.3, Berlin/Hong Kong, **2022**.
[27] W. K. Walter, D. E. Manolopoulos, R. G. Jones, *Surf. Sci.* **1996**, *348*, 115–132.
[28] I. A. Pašti, S. V. Mentus, *Electrochim. Acta* **2010**, *55*, 1995–2003.
[29] a) A. Baraldi, S. Lizzit, G. Comelli, M. Kiskinova, R. Rosei, K. Honkala, J. K. Nørskov, *Phys. Rev. Lett.* **2004**, *93*, 046101; b) A. Baraldi, *J. Phys. Condens. Matter* **2008**, *20*, 093001.

Manuscript received: July 21, 2023
Revised manuscript received: August 22, 2023
Accepted manuscript online: August 23, 2023
Version of record online: September 19, 2023